Journal of Solid State Chemistry 181 (2008) 3057–3064

Contents lists available at ScienceDirect

Journal of Solid State Chemistry

journal homepage: www.elsevier.com/locate/jssc

Crystallographic and infrared spectroscopic study of bond distances in $Ln[Fe(CN)_6]\cdot 4H_2O$ (Ln = lanthanide)

Xianju Zhou [a,b], Wing-Tak Wong [c], Michèle D. Faucher [d], Peter A. Tanner [b,*]

[a] Institute of Modern Physics, Chongqing University of Post and Telecommunications, Chongqing 400065, PR China
[b] Department of Biology and Chemistry, City University of Hong Kong, Tat Chee Avenue, Kowloon, Hong Kong SAR, PR China
[c] Department of Chemistry, The University of Hong Kong, Pokfulam Road, Pokfulam, Hong Kong SAR, PR China
[d] 308 Passage de la Creusaz, 74500 Neuvecelle, France

ARTICLE INFO

Article history:
Received 29 May 2008
Received in revised form
6 August 2008
Accepted 12 August 2008
Available online 17 August 2008

Keywords:
Bond distance
Lanthanide contraction
Infrared spectra
Crystal structure
Covalo-electrostatic model

ABSTRACT

Along with crystallographic data of $Ln[Fe(CN)_6]\cdot 4H_2O$ (Ln = lanthanide), the infrared spectra are reassigned to examine bond length trends across the series of Ln. The changes in mean Ln–O, Ln–N, C≡N and Fe–C distances are discussed and the bond natures of Ln–N and Ln–O are studied by bond length linear or quadratic fitting and comparisons with relevant ionic radii. The two different C≡N bond distances have been simulated by the covalo-electrostatic model.

1. Introduction

The series of bimetallic compounds $[(H_2O)2Ln(NC)6Fe]\cdot 2H_2O$ (Ln = lanthanide ion; written as $Ln[Fe(CN)_6]\cdot 4H_2O$ hereafter for brevity) have been the subject of numerous studies, partly because they are important precursors for the submicron perovskite-type oxides $LnFeO_3$ [1]. Their structural chemistry has a chequered history, with early reports identifying the crystal space group as monoclinic and with the structure of the Ln = Sm compound being mistaken for that of Ln = Er. In this study, the vibrational spectra of the $Ln[Fe(CN)_6]\cdot 4H_2O$ systems were reinvestigated not only because they have not been comprehensively studied previously, but also because there have been conflicting assignments. For example, Navarro et al. [2] assigned symmetric and antisymmetric CN stretching bands in $Nd[Fe(CN)_6]\cdot 4H_2O$ at 2135 and 2146 cm^{-1}, respectively. Xiaoyu et al. [3] assigned three bands at 1940, 2050 and 2140 cm^{-1} in this complex to CN stretching. One of the first two of these bands was alternatively assigned to the presence of Fe^{2+} [4], for which the CN stretch was reported at 2040 cm^{-1} in $(Pr/Nd)KFe(CN)_6\cdot 4H_2O$ [5]. Following our new vibrational assignments in the tetrahydrate systems, together with new crystallographic data for the Ln = Sm, Tb compounds, an investigation and rationalization of the Ln–NC–M bonding trends across the lanthanide series was possible, and comparisons with other $Ln[M^{III}(CN)_6]\cdot 4H_2O$ systems could be made. The major interest in bonding was to investigate the trends, especially for Ln–O and Ln–N bond distances, across the Ln^{3+} series and to observe evidence for deviations, if any, from ionic bonding. An orbital population analysis has been performed for C≡N bonds for comparison with experimental data.

2. Experimental

Solutions of $Ln[M(CN)_6]\cdot 4H_2O$ (M = Co, Fe) were prepared by mixing an aqueous solution of $Ln(NO_3)_3$ (prepared from the evaporation of a solution of concentrated HNO_3 and Ln_2O_3) together with an aqueous solution of $K_3M(CN)_6$. The mixture was filtered and left in the dark for crystals to form. Found (Calc.)% by mass for $PrCo(CN)_6\cdot 4H_2O$: C 16.825 (16.829), N 19.565 (19.633), H 1.890 (1.870). Other compounds were identified from their IR spectra. Nujol, fluorolube and KBr disk FTIR spectra were recorded at 2 cm^{-1} resolution over the range 400–4000 cm^{-1} using a Nicolet Avatar 360 instrument and gave similar results for a mull spectrum and for a KBr disk spectrum, as shown in Fig. 1(a) for $Sm[Fe(CN)_6]\cdot 4H_2O$. Single crystals were only obtained for $Ln[Fe(CN)_6]\cdot 4H_2O$ (Ln = Sm, Tb) and the other members of the series were prepared as powders. However, the spectra of

* Corresponding author. Fax: +86 852 2788 7406.
E-mail address: bhtan@cityu.edu.hk (P.A. Tanner).

0022-4596/$ - see front matter © 2008 Elsevier Inc. All rights reserved.
doi:10.1016/j.jssc.2008.08.008

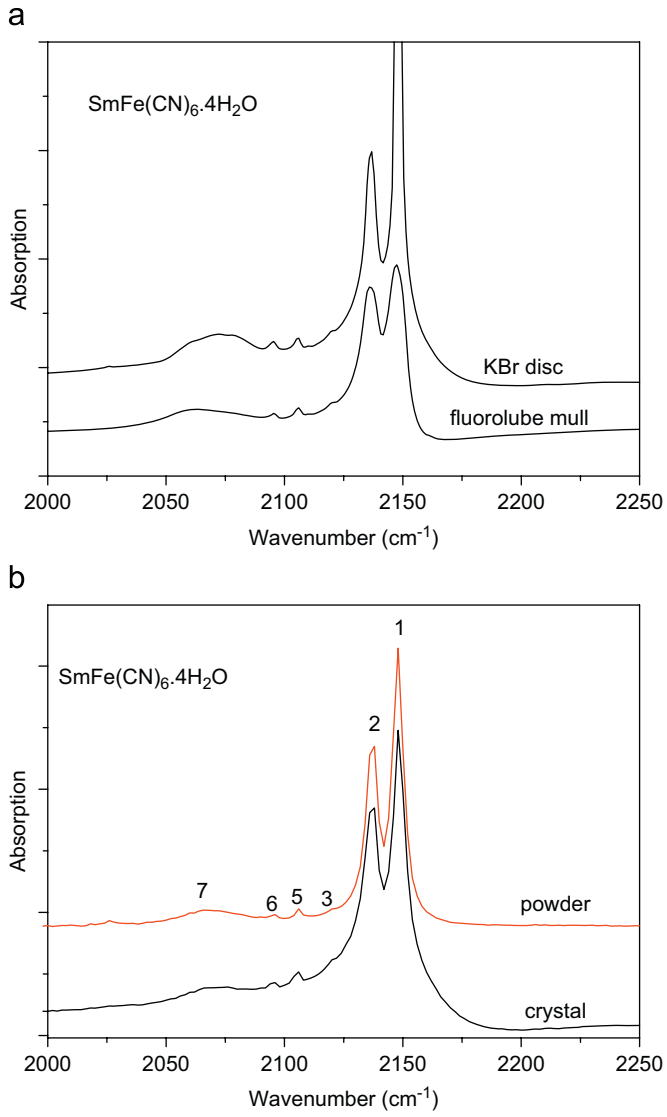

Fig. 1. (a) Comparison of fluorolube mull and KBr disk FTIR spectra of $Sm[Fe(CN)_6]\cdot 4H_2O$ and (b) FTIR spectra of KBr disks from powder or crystalline $Sm[Fe(CN)_6]\cdot 4H_2O$ forms. The bands are numbered as in Fig. 5.

preparations of powders and of single crystals subsequently ground up were similar, as shown in Fig. 1(b) for $Sm[Fe(CN)_6]\cdot 4H_2O$. Differential thermal absorption (DTA) and thermogravimetric (TG) results were obtained from room temperature to 550 °C using an SSC/5200 SII Seiko instrument, using a 10 °C min^{-1} heating rate and helium atmosphere.

X-ray determinations were carried out using a Bruker SMART CCD area detector with graphite monochromated Mo$K\alpha$ radiation as described in Table 1.

Table 1
Crystallographic data and parameters for $Ln[Fe(CN)_6]\cdot 4H_2O$ (Ln = Sm, Tb)

Empirical formula	$C_6H_8FeN_6O_4Tb$	$C_6H_8FeN_6O_4Sm$
Formula weight	434.41	442.94
Crystal color, habit	Red plate	Red rod
Crystal dimensions (mm)	0.01 × 0.01 × 0.02	0.01 × 0.01 × 0.09
Crystal system	Orthorhombic	Orthorhombic
Lattice type	C-centered	C-centered
Lattice parameters (Å) and volume (Å^3)	$a = 7.439(2)$	$a = 7.383(1)$
	$b = 12.874(2)$	$b = 12.828(2)$
	$c = 13.731(3)$	$C = 13.654(2)$
	$V = 1315.0(5)$	$V = 1293.2(3)$
Space group	*Cmcm* (no. 63)	*Cmcm* (#63)
Z	4	4
D_{calc} (g cm^{-3})	2.194	2.275
F_{000}	824.00	836.00
μ(Mo$K\alpha$) (cm^{-1})	55.489	65.49
Structure solution	Direct methods (SIR92)	Direct methods (SIR92)
Refinement	Full-matrix least squares on F	Full-matrix least-squares on F
Function minimized	$\Sigma w(\|F_o\|-\|F_c\|)^2$	$\Sigma w\ (\|F_o\|-\|F_c\|)^2$
Least-squares weights	$1/[0.0002F_o^2+\sigma(F_o^2)+0.005]$	$1/[0.0002F_o^2+\sigma(F_o^2)+0.006]$
$2\theta_{max}$ cutoff	55.0	55.0
Anomalous dispersion	All non-hydrogen atoms	All non-hydrogen atoms
No. observations ($I>2.00\sigma(I)$)	757	765
No. variables	57	57
Reflection/parameter ratio	13.28	13.42
Residuals: R ($I>2.00\sigma(I)$)	0.0288	0.0198
Residuals: R_w ($I>2.00\sigma(I)$)	0.0347	0.0237
Goodness of fit indicator	1.049	1.007
Max shift/error in final cycle	0.000	0.000
Maximum peak in final diff. map (e$^-$ Å^{-3})	0.98	1.15
Minimum peak in final diff. map (e$^-$ Å^{-3})	−0.89	−0.47

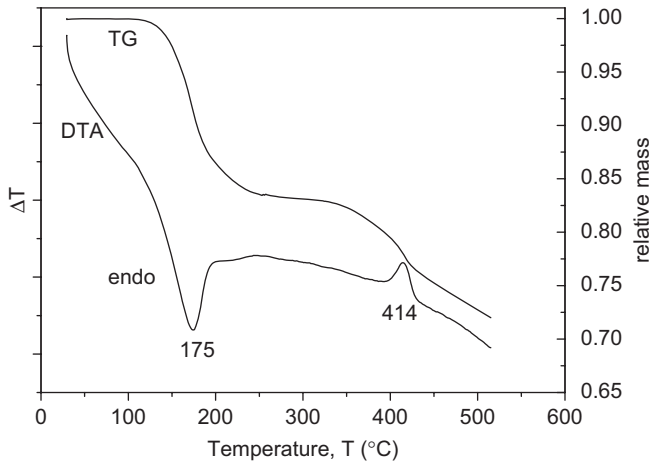

Fig. 2. Thermogravimetric (TG) and differential thermal absorption (DTA) plots for $Sm[Fe(CN)_6]\cdot 4H_2O$.

3. Results and discussion

3.1. Characterization of $Ln[M(CN)_6]\cdot 4H_2O$

Besides their different IR spectra [6], the clear distinction between the $Ln[M(CN)_6]\cdot xH_2O$ ($x = 4$ and 5) complexes can be made by the absence of the loss of one water molecule at a relatively low temperature. TG/DTA traces were taken for the series of compounds prepared and Fig. 2 shows a representative trace for Ln = Sm, M = Fe. In the helium atmosphere, the onset of mass loss is above 100 °C and by 300 °C about 17% of the mass has been lost, corresponding to the loss of $4H_2O$, following a major endothermic DTA peak at 175 °C and a weaker one at 217 °C. The DTA peaks for Ln = Eu, Gd, Er, Tm corresponding to that at 175 °C for Ln = Sm are at 165, 155, 144 and 141 °C, respectively. The exothermic event at 414 °C in Fig. 2 involves the decomposition of cyanide groups and the formation of carbonate. These results are in agreement with the previous thermal studies [1,3,7]. The IR

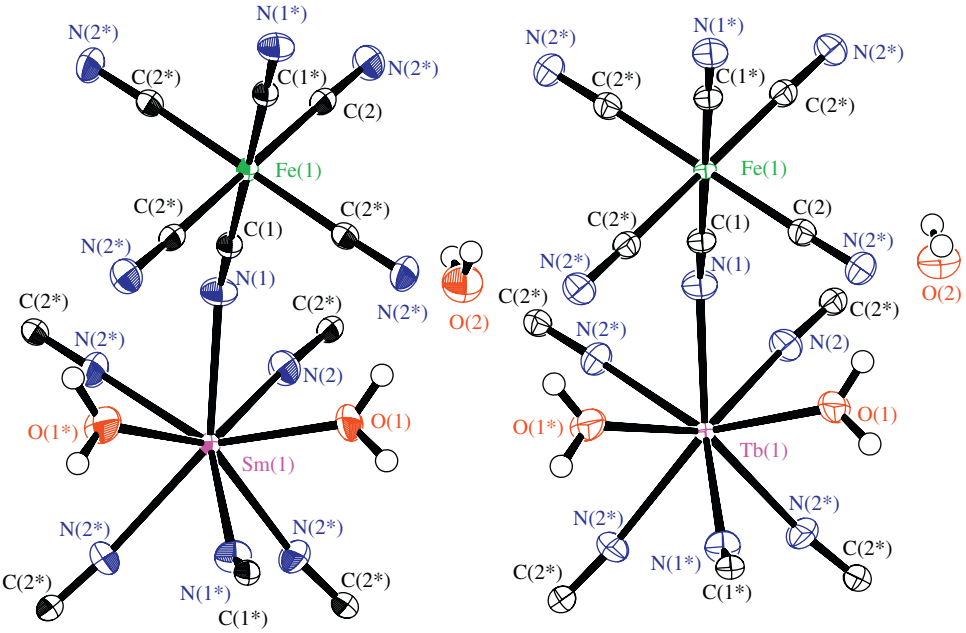

Fig. 3. Coordination geometry of $Sm[Fe(CN)_6]\cdot 4H_2O$ and $Tb[Fe(CN)_6]\cdot 4H_2O$.

spectra of the products of $Ln[Fe(CN)_6]\cdot 4H_2O$ after heating at 300 °C in air for 12 h show the absence of cyanide groups and the presence of nitrate and carbonate. In summary, both the IR and TG results have confirmed that the prepared samples are tetrahydrates.

3.2. Crystal structures

The crystal structures of the isomorphous compounds $Ln[Fe(CN)_6]\cdot 4H_2O$ where $Ln = Sm$, Tb have been determined herein. Fig. 3 shows the coordination geometry of the $Ln = Tb$, Sm compounds, which crystallize in the orthorhombic space group *Cmcm*, $Z = 4$. The crystallographic data are summarized in Table 1 and selected bond lengths and angles are given in Tables 2 and 3. The Tb^{3+} ion in $Tb[Fe(CN)_6]\cdot 4H_2O$ is eight-coordinated in square antiprismatic geometry to six N atoms of six CN ligands, as well as to two O atoms of aqua ligands. The C atoms of the CN groups are bonded to Fe^{3+} ions. The uncoordinated zeolitic water molecules are hydrogen-bonded to one of the N atoms of the $Fe(CN)_6$ groups. Views of the packing diagrams of $Sm[Fe(CN)_6]\cdot 4H_2O$ are shown in Fig. 4. The two crystal structures are in agreement with those previously published for $Ln[Fe(CN)_6]\cdot 4H_2O$, $Ln =$ Nd [2], Sm [8], Gd [9], Er [10,11].

3.3. Infrared spectra in the C≡N stretching region

Fig. 5 shows the FTIR spectra of KBr disks of $Tb[Fe(CN)_6]\cdot 4H_2O$ in the CN stretching region. The strong bands marked 1 (at 2151 cm^{-1}) and 2 (at 2140 cm^{-1}) in the figure, with band 1 being more intense, are $^{12}C^{14}N$ stretching bands of the bridged Tb–N≡C–Fe system. These are labeled CN(a) and CN(b), respectively. The very weak bands marked 3 (at 2121 cm^{-1}) and 4 (at 2114 cm^{-1}) are $^{12}C^{15}N$ stretching bands, whereas those labeled 5 (at 2108 cm^{-1}) and 6 (at 2098 cm^{-1}) are $^{13}C^{14}N$ stretching bands. The broad feature labeled 7, with maximum intensity at 2066 cm^{-1}, which has previously been assigned to a CN stretch [3] or a difference band [6], is alternatively assigned to a combination band due to the prominent water bending modes (at 1608 and 1683 cm^{-1} in the IR spectrum) and the Fe–C stretch (423 ± 2 cm^{-1}).

Fig. 6 shows a plot of the two CN stretching frequencies against the Shannon ionic radius of Ln^{3+} for this series of complexes and a smooth increase is observed across the Ln^{3+} series from Pr to Yb. These vibrations can be regarded as characteristic group frequencies, which are not mixed with other vibrations. The increase thus indicates slightly shorter C≡N bond distances for the later *Ln* members, but the overall change in vibration frequency is <2%. Since *M* is constant, this small change must be attributed solely to the variation of *Ln*. The reported plot of CN stretching frequencies versus ionic radius for $Ln[Au(CN)_2]_3\cdot 3H_2O$ complexes [12] exhibits a similar trend to Fig. 6 although the two ν(C≡N) stretching frequencies are at a rather higher energy since the CN bond distance is shorter [N(1)–C(1) 109(3) pm].

3.4. Mean bond distances in $Ln[M(CN)_6]\cdot 4H_2O$

It is interesting to probe the changes in bond distances in the *Ln*–N≡C–Fe system, which arise solely by changing the nature of *Ln*. In this section, our crystallographic data for $Ln[Fe(CN)_6]\cdot 4H_2O$, $M =$ Sm, Tb are combined with those previously published for $Ln =$ Nd, Gd, Er systems in order to draw conclusions concerning *average* bond distances.

For the transition metal, *M*, in the *Ln*–N≡C–*M* system, the $C\equiv N^-$ ligand acts as a base by donating HOMO 3σ electrons and as a weak acid by accepting electrons into the 2π LUMO. This behavior parallels that of CO and it is the d_{x2-y2} and d_{z2} orbitals of M^{3+} that are suitably oriented for overlap with the π^* antibonding orbital of the ligand [13]. It is generally thought that such a back-donation will weaken the C≡N bond and shorten *M*–C. On comparing the scenario for $Sm[Fe(CN)_6]\cdot 4H_2O$ with that for $Sm[Co(CN)_6]\cdot 4H_2O$, where crystallographic data are available [14], the Fe complex does have a longer *M*–C distance (by 3.8 pm), and also longer CN distance (by 1.2 pm). The general interpretation for such phenomena [15] due to changes in *d*-block elements, *M*, is that the *M*–CN σ bonding increases with the number of *d*-electrons, but that increasing the effective nuclear

Table 2
Selected bond lengths and bond angles for $Sm[Fe(CN)_6]\cdot 4H_2O$

Atom	Atom	Distance	Atom	Atom	Distance
Bond lengths (Å)					
Sm(1)	O(1)	2.400(6)	Sm(1)	$O(1)^{1)}$	2.400(6)
Sm(1)	N(1)	2.533(6)	Sm(1)	$N(1)^{2)}$	2.533(6)
Sm(1)	N(2)	2.499(4)	Sm(1)	$N(2)^{1)}$	2.499(4)
Sm(1)	$N(2)^{2)}$	2.499(4)	Sm(1)	$N(2)^{3)}$	2.499(4)
Fe(1)	C(1)	1.926(6)	Fe(1)	$C(1)^{4)}$	1.926(6)
Fe(1)	C(2)	1.932(5)	Fe(1)	$C(2)^{1)}$	1.932(5)
Fe(1)	$C(2)^{4)}$	1.932(5)	Fe(1)	$C(2)^{5)}$	1.932(5)
O(1)	H(1)	0.904	O(1)	$H(1)^{3)}$	0.904
O(2)	H(2)	0.863	O(2)	H(3)	0.916
N(1)	C(1)	1.151(9)	N(2)	$C(2)^{6)}$	1.155(7)
Symmetry operators					
(1)−*X*+1,*Y*,*Z*			(2)−*X*+1,*Y*,−*Z*+1/2		
(3)*X*,*Y*,−*Z*+1/2			(4)−*X*+1,−*Y*+1,−*Z*+1		
(5)*X*,−*Y*+1,−*Z*+1			(6)−*X*+1/2,−*Y*+1/2,−*Z*+1		

Atom	Atom	Atom	Angle	Atom	Atom	Atom	Angle
Bond angles (deg)							
O(1)	Sm(1)	$O(1)^{1)}$	109.4(2)	O(1)	Sm(1)	N(1)	71.64(10)
O(1)	Sm(1)	$N(1)^{2)}$	71.64(10)	O(1)	Sm(1)	N(2)	78.86(16)
O(1)	Sm(1)	$N(2)^{1)}$	142.45(11)	O(1)	Sm(1)	$N(2)^{2)}$	142.45(11)
O(1)	Sm(1)	$N(2)^{3)}$	78.86(16)	$O(1)^{1)}$	Sm(1)	N(1)	71.64(10)
$O(1)^{1)}$	Sm(1)	$N(1)^{2)}$	71.64(10)	$O(1)^{1)}$	Sm(1)	N(2)	142.45(11)
$O(1)^{1)}$	Sm(1)	$N(2)^{1)}$	78.86(16)	$O(1)^{1)}$	Sm(1)	$N(2)^{2)}$	78.86(16)
$O(1)^{1)}$	Sm(1)	$N(2)^{3)}$	142.45(11)	N(1)	Sm(1)	$N(1)^{2)}$	113.9(2)
N(1)	Sm(1)	N(2)	77.04(15)	N(1)	Sm(1)	$N(2)^{1)}$	77.04(15)
N(1)	Sm(1)	$N(2)^{2)}$	142.19(11)	N(1)	Sm(1)	$N(2)^{3)}$	142.19(11)
$N(1)^{2)}$	Sm(1)	N(2)	142.19(11)	$N(1)^{2)}$	Sm(1)	$N(2)^{1)}$	142.19(11)
$N(1)^{2)}$	Sm(1)	$N(2)^{2)}$	77.04(15)	$N(1)^{2)}$	Sm(1)	$N(2)^{3)}$	77.04(15)
N(2)	Sm(1)	$N(2)^{1)}$	74.32(16)	N(2)	Sm(1)	$N(2)^{2)}$	117.49(15)
N(2)	Sm(1)	$N(2)^{3)}$	74.45(15)	$N(2)^{1)}$	Sm(1)	$N(2)^{2)}$	74.45(15)
$N(2)^{1)}$	Sm(1)	$N(2)^{3)}$	117.49(15)	$N(2)^{2)}$	Sm(1)	$N(2)^{3)}$	74.32(16)
C(1)	Fe(1)	$C(1)^{4)}$	180.0(2)	C(1)	Fe(1)	C(2)	89.0(2)
C(1)	Fe(1)	$C(2)^{1)}$	89.0(2)	C(1)	Fe(1)	$C(2)^{4)}$	91.0(2)
C(1)	Fe(1)	$C(2)^{5)}$	91.0(2)	$C(1)^{4)}$	Fe(1)	C(2)	91.0(2)
$C(1)^{4)}$	Fe(1)	$C(2)^{1)}$	91.0(2)	$C(1)^{4)}$	Fe(1)	$C(2)^{4)}$	89.0(2)
$C(1)^{4)}$	Fe(1)	$C(2)^{5)}$	89.0(2)	C(2)	Fe(1)	$C(2)^{1)}$	90.8(2)
C(2)	Fe(1)	$C(2)^{4)}$	0(440)	C(2)	Fe(1)	$C(2)^{5)}$	89.2(2)
$C(2)^{1)}$	Fe(1)	$C(2)^{4)}$	89.2(2)	$C(2)^{1)}$	Fe(1)	$C(2)^{5)}$	0(440)
$C(2)^{4)}$	Fe(1)	$C(2)^{5)}$	90.8(2)	Sm(1)	O(1)	H(1)	130.5
Sm(1)	O(1)	$H(1)^{3)}$	130.5	H(1)	O(1)	$H(1)^{3)}$	98.9
H(2)	O(2)	H(3)	119.9	Sm(1)	N(1)	C(1)	149.0(5)
Sm(1)	N(2)	$C(2)^{6)}$	167.1(4)	Fe(1)	C(1)	N(1)	178.8(6)
Fe(1)	C(2)	$N(2)^{6)}$	178.2(4)				
Symmetry operators							
(1)−*X*+1,*Y*,*Z*				(2)−*X*+1,*Y*,−*Z*+1/2			
(3)*X*,*Y*,−*Z*+1/2				(4)−*X*+1,−*Y*+1,−*Z*+1			
(5)*X*,−*Y*+1,−*Z*+1				(6)−*X*+1/2,−*Y*+1/2,−*Z*+1			

charge on *M* stabilizes the *d* orbitals to a greater extent so that $d\pi$–$p\pi^*$ *M*–CN backbonding occurs to a smaller extent.

The Fe–C bond distances (R_{Fe-C}) are not determined accurately for this series of compounds and there is scatter across the series, although there is an overall increase from *Ln* = Nd (189.9 pm) to *Ln* = Er (193.8 pm) of 3.9 nm. The regression with atomic number (*Z*) of *Ln* gives $R_{Fe-C} = 166.4+0.411Z$, $N = 5$, $R^2 = 0.649$. The IR active Fe–C stretching frequency [ν(Fe–C)] only changes slightly from *Ln* = Pr to Yb (mean value 423.8 cm^{-1}; standard deviation 1.4 cm^{-1}; $N = 10$). Linear regression of ν(Fe–C) against R_{Fe-C} gives $\nu(Fe-C) = 226.6+1.023\ R_{Fe-C}$, $N = 5$, $R^2 = 0.752$, which suggests an increase in frequency with increasing bond distance. However, since the variation in vibrational frequency is very small and the frequency is low, the changes could arise from other factors such as mode mixing rather than bond length changes. The *M*–C bond distance has been shown to be particularly sensitive to the nature of *M* in $Pr[M(CN)_6]\cdot 5H_2O$ (*M* = Cr, Fe, Co) [16].

The mean value of the C≡N bond distances for these five compounds is 115.6 pm (standard deviation 0.4 pm), which is the same bond distance as the literature value for C≡N. It is more sensitive to probe variations in the mean C≡N distance by vibrational stretching frequencies as in the previous section.

The variation in the mean *Ln*–N and *Ln*–O distances across the series of *Ln* is now considered. The maximum error in the crystallographically determined *Ln*–O and *Ln*–N distances is ~0.2%. Plotting the bond distance of sodium halides versus atomic number leads to a linear plot that can be taken as the representative of ionic bonding. If the *Ln*–O bonding is envisaged as ionic in character then there should be a similar trend in this distance to that for the sum of the Shannon Ln^{3+}(VIII) and O^{2-}(III) ionic radii. On combining our crystallographic data with those from previous studies, it is found that the variation in the determined *Ln*–O distances with atomic number of *Ln* can in fact be fitted for five compounds with a higher adjusted R^2 value by a

Table 3
Selected bond lengths and bond angles for $Tb[Fe(CN)_6]\cdot 4H_2O$

Atom	Atom	Distance	Atom	Atom	Distance
Bond lengths (Å)					
Tb(1)	O(1)	2.355(3)	Tb(1)	$O(1)^{1)}$	2.355(3)
Tb(1)	N(1)	2.489(4)	Tb(1)	$N(1)^{2)}$	2.489(4)
Tb(1)	N(2)	2.461(2)	Tb(1)	$N(2)^{1)}$	2.461(2)
Tb(1)	$N(2)^{2)}$	2.461(2)	Tb(1)	$N(2)^{3)}$	2.461(2)
Fe(1)	C(1)	1.928(4)	Fe(1)	$C(1)^{4)}$	1.928(4)
Fe(1)	C(2)	1.935(3)	Fe(1)	$C(2)^{1)}$	1.935(3)
Fe(1)	$C(2)^{4)}$	1.935(3)	Fe(1)	$C(2)^{5)}$	1.935(3)
O(1)	H(1)	0.838	O(1)	$H(1)^{3)}$	0.838
O(2)	H(2)	0.915	O(2)	H(3)	0.763
N(1)	C(1)	1.157(5)	N(2)	$C(2)^{6)}$	1.153(4)
Symmetry operators					
(1)−*X*+1,*Y*,*Z*			(2)−*X*+1,*Y*,−*Z*+1/2		
(3)*X*,*Y*,−*Z*+1/2			(4)−*X*+1,−*Y*+1,−*Z*+1		
(5)*X*,−*Y*+1,−*Z*+1			(6)−*X*+1/2,−*Y*+1/2,−*Z*+1		

Atom	Atom	Atom	Angle	Atom	Atom	Atom	Angle
Bond angles (deg)							
O(1)	Tb(1)	$O(1)^{1)}$	109.91(13)	O(1)	Tb(1)	N(1)	71.60(6)
O(1)	Tb(1)	$N(1)^{2)}$	71.60(6)	O(1)	Tb(1)	N(2)	78.63(10)
O(1)	Tb(1)	$N(2)^{1)}$	142.26(7)	O(1)	Tb(1)	$N(2)^{2)}$	142.26(7)
O(1)	Tb(1)	$N(2)^{3)}$	78.63(10)	$O(1)^{1)}$	Tb(1)	N(1)	71.60(6)
$O(1)^{1)}$	Tb(1)	$N(1)^{2)}$	71.60(6)	$O(1)^{1)}$	Tb(1)	N(2)	142.26(7)
$O(1)^{1)}$	Tb(1)	$N(2)^{1)}$	78.63(10)	$O(1)^{1)}$	Tb(1)	$N(2)^{2)}$	78.63(10)
$O(1)^{1)}$	Tb(1)	$N(2)^{3)}$	142.26(7)	N(1)	Tb(1)	$N(1)^{2)}$	113.32(13)
N(1)	Tb(1)	N(2)	77.10(9)	N(1)	Tb(1)	$N(2)^{1)}$	77.10(9)
N(1)	Tb(1)	$N(2)^{2)}$	142.32(7)	N(1)	Tb(1)	$N(2)^{3)}$	142.32(7)
$N(1)^{2)}$	Tb(1)	N(2)	142.32(7)	$N(1)^{2)}$	Tb(1)	$N(2)^{1)}$	142.32(7)
$N(1)^{2)}$	Tb(1)	$N(2)^{2)}$	77.10(9)	$N(1)^{2)}$	Tb(1)	$N(2)^{3)}$	77.10(9)
N(2)	Tb(1)	$N(2)^{1)}$	74.23(9)	N(2)	Tb(1)	$N(2)^{2)}$	117.75(9)
N(2)	Tb(1)	$N(2)^{3)}$	74.78(9)	$N(2)^{1)}$	Tb(1)	$N(2)^{2)}$	74.78(9)
$N(2)^{1)}$	Tb(1)	$N(2)^{3)}$	117.75(9)	$N(2)^{2)}$	Tb(1)	$N(2)^{3)}$	74.23(9)
C(1)	Fe(1)	$C(1)^{4)}$	180.00(18)	C(1)	Fe(1)	C(2)	91.01(12)
C(1)	Fe(1)	$C(2)^{1)}$	91.01(12)	C(1)	Fe(1)	$C(2)^{4)}$	88.99(12)
C(1)	Fe(1)	$C(2)^{5)}$	88.99(12)	$C(1)^{4)}$	Fe(1)	C(2)	88.99(12)
$C(1)^{4)}$	Fe(1)	$C(2)^{1)}$	88.99(12)	$C(1)^{4)}$	Fe(1)	$C(2)^{4)}$	91.01(12)
$C(1)^{4)}$	Fe(1)	$C(2)^{5)}$	91.01(12)	C(2)	Fe(1)	$C(2)^{1)}$	90.66(13)
C(2)	Fe(1)	$C(2)^{4)}$	180.00(18)	C(2)	Fe(1)	$C(2)^{5)}$	89.34(13)
$C(2)^{1)}$	Fe(1)	$C(2)^{4)}$	89.34(13)	$C(2)^{1)}$	Fe(1)	$C(2)^{5)}$	180.00(18)
$C(2)^{4)}$	Fe(1)	$C(2)^{5)}$	90.66(13)	Tb(1)	O(1)	H(1)	127.2
Tb(1)	O(1)	$H(1)^{3)}$	127.2	H(1)	O(1)	$H(1)^{3)}$	102.6
H(2)	O(2)	H(3)	124.8	Tb(1)	N(1)	C(1)	149.8(3)
Tb(1)	N(2)	$C(2)^{6)}$	167.5(2)	Fe(1)	C(1)	N(1)	178.7(4)
Fe(1)	C(2)	$N(2)^{7)}$	178.4(2)				
Symmetry operators							
(1)−*X*+1,*Y*,*Z*				(2)−*X*+1,*Y*,−*Z*+1/2			
(3)*X*,*Y*,−*Z*+1/2				(4)−*X*+1,−*Y*+1,−*Z*+1			
(5)*X*,−*Y*+1,−*Z*+1				(6)−*X*+1/2,*Y*+1/2−1,*Z*			
(7)−*X*+1/2,*Y*+1/2,*Z*							

polynomial for which the dominant term is the quadratic term: $Ln\text{–O} = 682.4-12.36Z+0.0844Z^2$ ($R^2(\text{adj}) = 0.9965$) than by a linear fit ($R^2(\text{adj}) = 0.9714$). This could be taken to indicate a deviation from purely ionic bonding. However, the fit of the sum of the Shannon ionic radii versus Z can be fitted almost equally well by a linear fit ($R^2(\text{adj}) = 0.9923$) or the quadratic relation: $[Ln^{3+}(\text{VIII})+O^{2-}(\text{III})] = 428.0-4.56Z+0.0256Z^2$ ($R^2(\text{adj}) = 0.9965$). What is more pertinent is that there is a larger discrepancy between the two curves for the latter, rather than the earlier, members of *Ln* (i.e., the *Ln*–O distances deviate more from the sum of ionic radii) since the smaller cations are more polarizing and some degree of participation of 4*f*, 5*d* or 6*s* orbitals in bonding is suggested. Angelov [17] has calculated the overlap integrals for the series Ln_2O_3 and concluded that only π-type (and not σ-type) delocalization is possible and that the $2p\pi$–4*f* overlap integrals are greater for the early lanthanides. A plot of the *Ln*–O bond distances for the C_2 site symmetry Ln^{3+} versus lanthanide atomic number from his data is similarly fitted by a straight line ($R^2(\text{adj}) = 0.983$) or by a quadratic function ($R^2(\text{adj}) = 0.989$).

Finally, it is noted that the mean *Ln*–O distances are slightly longer (0.5–1.7 pm) in $Ln[Fe(CN)_6]\cdot 4H_2O$ than in $Ln[Co(CN)_6]\cdot 4H_2O$, *Ln* = Nd [18], Sm [14], Er [19] where the ionic radius of Fe^{3+} is 3 pm longer than that of Co^{3+}.

From the plot of mean *Ln*–N distance in $Ln[Fe(CN)_6]\cdot 4H_2O$ against Z, the linear regression line is $Ln\text{–N} = 348.4-1.562Z$ ($R^2(\text{adj}) = 0.9914$) and the quadratic regression line has $R^2(\text{adj}) = 0.9876$. On the other hand, the plot of Shannon ionic radii $[Ln^{3+}(\text{VIII})+N^{3-}(\text{IV})]\cdot$ versus Z has the following quadratic relation: $[Ln^{3+}(\text{VIII})+N^{3-}(\text{IV})] = 438.0-4.56Z+0.0256Z^2$ ($R^2(\text{adj}) = 0.9965$), whereas the linear fit has $R^2(\text{adj}) = 0.9923$. This time, the *Ln*–N versus Z plot can be fitted slightly better by a linear equation and again, the deviation of the *Ln*–N versus Z plot from the $[Ln^{3+}(\text{VIII})+N^{3-}(\text{IV})]\cdot$ versus Z plot is more evident for the later members of *Ln*. The mean *Ln*–N bond distance (e.g., 247.0 pm for

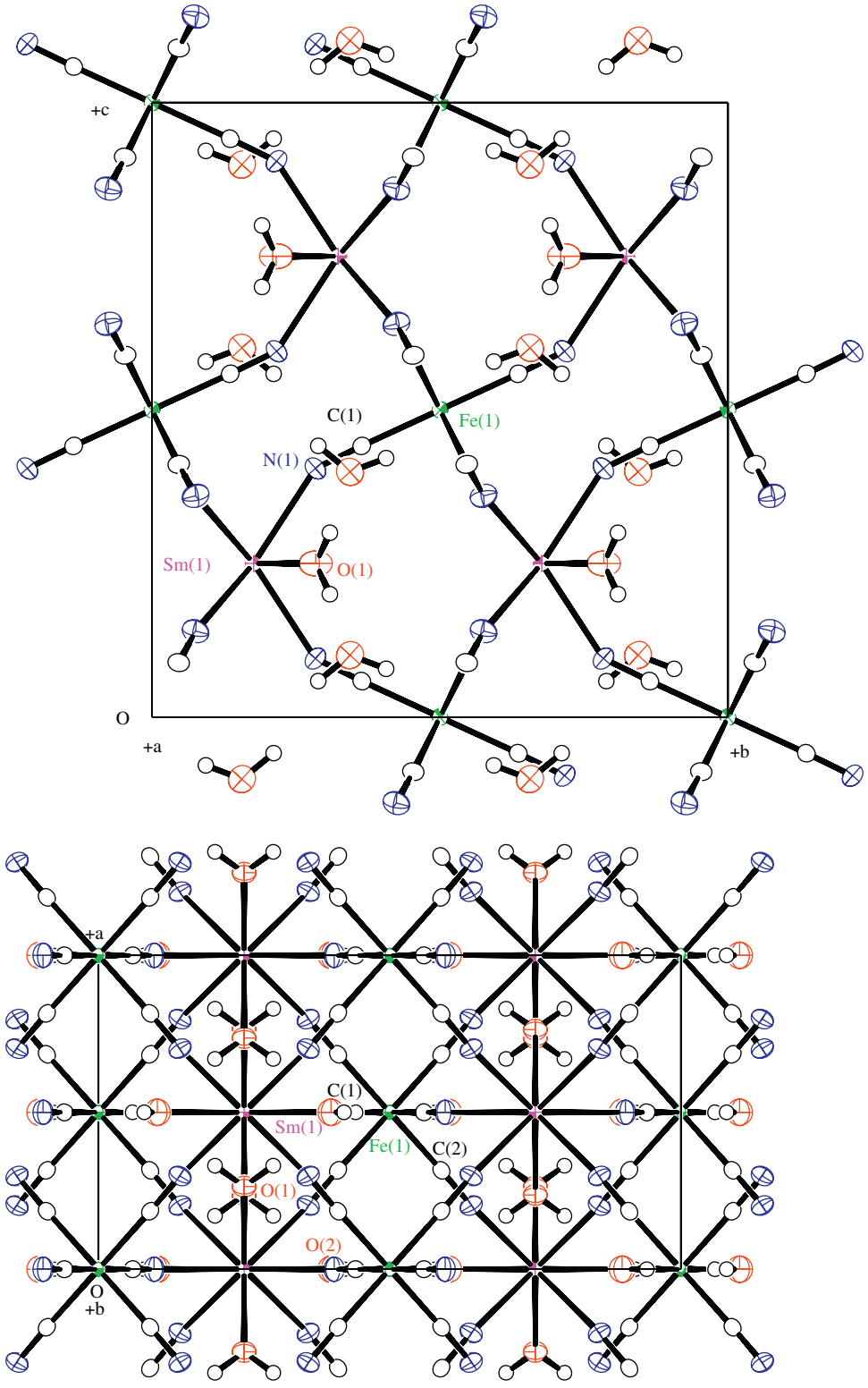

Fig. 4. Packing diagram of $Sm[Fe(CN)_6] \cdot 4H_2O$ projected along the *a*- and *b*-axis of the unit cell.

Ln = Tb) is much longer than the 209.1 pm reported for the *Lu*–N bond in a lutetium imido complex [20].

3.5. Model calculations of individual bond distances

Fig. 7 shows the 8-fold close environment of the rare earth with two O(1), two N(1) and four N(2) ligands forming a nearly regular square antiprism (note that the definitions of *N*(1) and N(2) on the one hand, and O(1) and O(2) on the other, are interchanged when following different authors). The four coplanar N(2) form a square. The two N(1) and the two O(1) are nearly coplanar ($\Delta z = 1.5$ pm) and form a distorted square. The point group at the rare-earth site is C_{2v}. As shown in Fig. 7, the crystallographic O*y*-axis (b) is the O*z*-axis of the point group at the

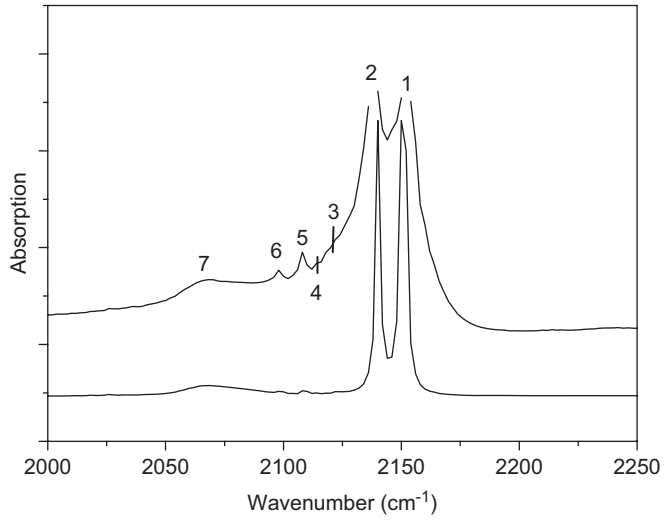

Fig. 5. Infrared spectra between 2000 and 2200 cm^{-1} of KBr disks of samples of $Tb[Fe(CN)_6]\cdot 4H_2O$. The numbered bands 1–7 are assigned in the text. The top curve is the spectrum of a more concentrated sample, whose bands 3–7 are more obvious.

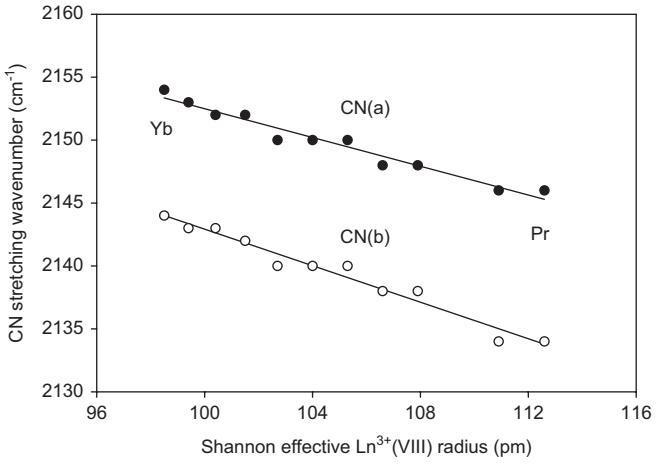

Fig. 6. Plot of the two CN stretching frequencies (labeled CN(a) and CN(b)) against the Shannon ionic radius of Ln^{3+}(VIII) (S_R) for $Ln[Fe(CN)_6]\cdot 4H_2O$. The error in wavenumber is $\pm 1\,cm^{-1}$ and values are given to the nearest integer. The linear regression lines ($N = 11$) are drawn: $CN(a) = 2210 - 0.571S_R$ ($R^2 = 0.9592$) and $CN(b) = 2215 - 0.725S_R$ ($R^2 = 0.9672$). Alternatively, linear regression against atomic number, Z, gives $CN(a) = 2079 - 0.9279Z$ ($R^2 = 0.9575$) and $CN(b) = 2102 - 0.7391Z$ ($R^2 = 0.9714$). Note the differences in the zero intercepts for the S_R and Z plots and that although CN(a) is higher than CN(b) it gives lower intercepts.

Ln site. The nitrogen atoms are bonded to carbon atoms at about 115 pm: the two N(1) and the four N(2) are bonded to two C(1) and four (C2), respectively. Six *Ln*–N≡C–Fe threads pointing outwards ensure the bonding with the rest of the structure. The nearest O(2) is at 474 pm from the rare earth in the terbium compound. The smallest N(1)–O(2) distance is 282 pm. Therefore, it is considered that O(2) has a minor influence on the bonding close to the rare earth.

From the five complete structural determinations made for $Ln[Fe(CN)_6]\cdot 4H_2O$, Fig. 8 represents, as a function of Z, the nearest metal–ligand distance for the three crystallographic species O(1), N(1) and N(2). The *Ln*–O(1), *Ln*–N(1) and *Ln*–N(2) distances regularly decrease along the rare-earth series as a consequence of the lanthanide contraction. It is worth noting that the *Ln*–N(1) (e.g., Tb–N(1) 248.9(0.4) pm) is larger than the *Ln*–N(2) (e.g., Tb–N(2) 246.1(0.3) pm) distance.

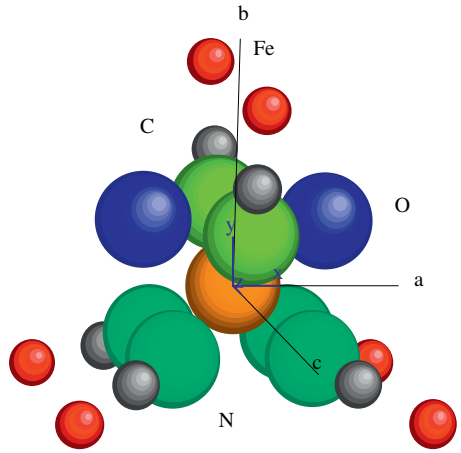

Fig. 7. The 8-fold close environment of the rare earth with two O(1), two N(1) and four N(2) ligands.

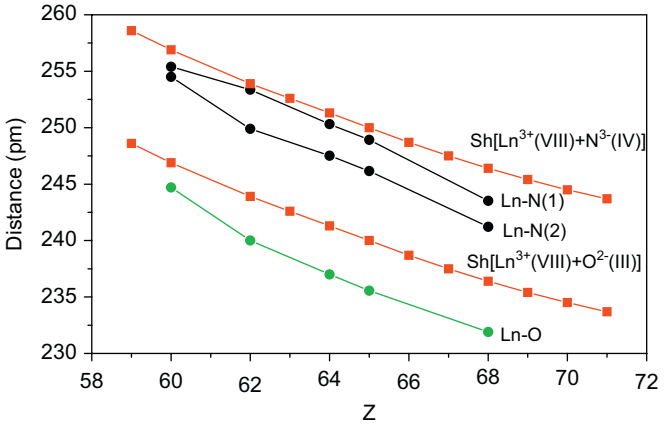

Fig. 8. Bond distances in $Ln[Fe(CN)_6]\cdot 4H_2O$ versus atomic number. Squares represent sums of Shannon ionic radii. Top circles are for *Ln*–N(1) and *Ln*–N(2) bonds. Lower circles represent *Ln*–O bonds. The lines are a guide to the eye. In Table 1 of [9], the *z*-coordinate of N(1) should be 0.1405 instead of 0.1505.

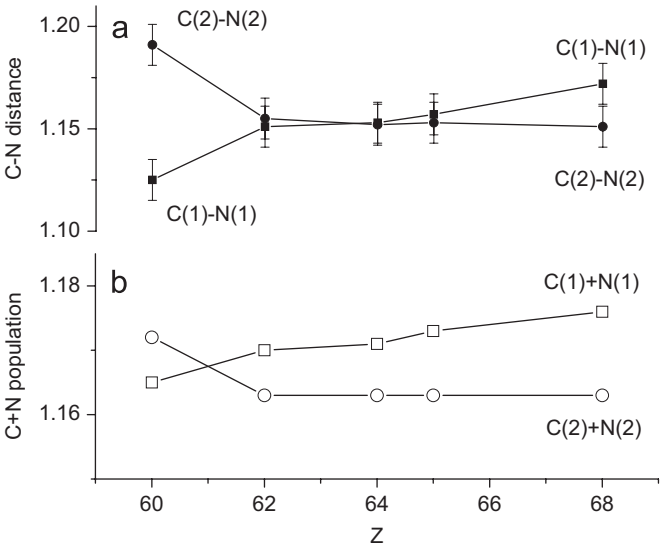

Fig. 9. (a) Variation of the C(1)–N(1) and C(2)–N(2) distances along the series $Ln[Fe(CN)_6]\cdot 4H_2O$ from crystallographic data and (b) calculated C+N populations from the covalo-electrostatic model.

Fig. 9(a) shows the variation of the C(1)–N(1) and C(2)–N(2) distances along the series. Although the determination is not precise, the trend is definitely an increase of the C(1)–N(1) distance and a lowering of the C(2)–N(2) distance along the series. The explanation of these two experimental observations can be sought for in the change of the electronic population of C(1) and N(1) on the one hand, and of C(2) and N(2) on the other. To evaluate the change, a *covalo-electrostatic model* [21] was utilized. In the model, the interactions within a cluster are limited to the free-ion orbital energies, the coulombic diagonal interaction terms and the kinetic energy off-diagonal terms. A cluster consisting of the *Ln* central ion, two oxygens, six nitrogens and six carbon atoms was considered (i.e., the atoms represented in Fig. 7 except for the iron atoms). Only the valence shells of the 15 atoms, 4*f* for *Ln* and 2*p* for the other atoms, are taken into account. The total number of orbitals (three for O, N and C, seven for *Ln*) amounts to 49 and represents the dimension of the interaction matrix. The ionization energies and the basis sets of Slater-type orbitals for Sm^{3+}, Tb^{3+} and Er^{3+} are given in [22], and those for O^{2-}, N and C in [23]. The interactions between all close neighbors *Ln*–O(1), *Ln*–N(1), *Ln*–N(2), *C*(1)–N(1) and *C*(2)–*N*(2) were calculated. Actually, it is difficult to evaluate the coulombic diagonal interaction terms for nitrogen and carbon, which are not fully ionized. Therefore, the results of Teng and Wu [24], considering the electronic spectra of $C_{76}N_2$ isomers, were utilized. These authors determine the LUMO–HOMO energy gaps for the closed-shell $C_{76}N_2$ isomers as equal to 3.4578 eV (27887 cm^{-1}) for the most stable isomer. In this way, the difficult point consisting in the determination of the energetic positions of C and N atoms is partially solved. The starting values for the ionization energies were (in cm^{-1}) as follows: −100,000, −135,000, −94,473 (value for neutral carbon given in [23]), and −122,360, for Ln^{3+}, O^{2-}, C and N, respectively.

The diagonalization of the interaction matrix provided the wave vectors of the system, allowing for the evaluation of the approximate population on each orbital. The *Ln* and O(1) orbitals retain 99% of their initial population. N(1) and N(2), drastically mixed with C(1) and C(2), share grossly half of their population (Fig. 8). It was assumed that the sum of the Mulliken populations of C(1) and N(1) on the one hand, and of C(2) and N(2) on the other, follow the variation of the C(1)–N(1) and C(2)–N(2) distances. The ionization energies of N(1), N(2), C(1) and C(2) were tuned until the two following conditions were obeyed as well as possible: the *Ln*–N(1) distance is larger than the *Ln*–N(2) distance and the variation of the C(1)–N(1) and C(2)–N(2) distances matches that represented in Fig. 9(a). The best results were obtained for ionization energies equal (in cm^{-1}) to −122,905, −116,905, −94,373 and −90,373 for N(1), N(2), C(1) and C(2), respectively. Fig. 9(b) shows the variation of the C(1)+N(1) and the C(2)+N(2) populations and is to be compared with the experimental values shown in Fig. 9(a).

4. Conclusions

A quadratic variation of bond distances with atomic number has previously been found in $[Ln(OH_2)_9][C_2H_5OSO_3]_3$ for *Ln*–O bonds [25], and in $CsLnZnTe_3$ for *Ln*–Te distances [26]. The formula $d(Ln\text{–}X) = A_0 - A_1 n + A_2^2 n^2$ (where n = number of *f*-electrons) given in the former case to represent the lanthanide contraction also has the terms A_0, A_1, A_2 decreasing by two orders from one to the next. In the present case, the quadratic fit for *Ln*–O bond distances is marginally better than a linear fit, but the linear fit is slightly better for *Ln*–N bond distances. The quadratic evolution could be taken as an indication of some lanthanide valence orbital participation along the series, notably for the late members where the difference from the sums of Shannon ionic radii is greatest. However, the covalent effects are very small and more crystallographic data for this system from other *Ln* would provide more accurate fits. The variation in C–N bond distances across the $Ln[Fe(CN)_6]\cdot 4H_2O$ series from *Ln* = Nd to Er has been simulated by the covalo-electrostatic model.

Both the usual σ and π^* $C\equiv N^-$ bonding mechanisms would be expected to lead to weaker CN bonds for shorter *Ln*–O distances, as expected for a donor–acceptor interaction, but the IR spectral evidence shows that this does not happen. Thus, it is concluded that on traversing across the lanthanide series for $Ln[Fe(CN)_6]\cdot 4H_2O$, there are decreases in *Ln*–N and *Ln*–O bond distances and slight changes, perhaps also decreases, in CN distances.

Supplementary data

Crystallographic information for $Ln[Fe(CN)_6]\cdot 4H_2O$ is available as CCDC652090 (*M* = Sm) and CCDC652091 (*M* = Tb) from the Cambridge Crystallographic Data Centre (CCDC). These data may be obtained free of charge from the CCDC via the web link www.ccdc.cam.ac.uk/data_request/cif.

Acknowledgment

Financial support of this work by the Hong Kong University Grants Commission Earmarked Research Grant CityU 102607 is gratefully acknowledged. X.J. acknowledges the financial support from the National Natural Science Foundation of China (Grant no. 10704090). We thank Dr. Dominique Guillaumont for preliminary calculations and for drawing our attention to Refs. [25,26].

References

[1] Y. Sadaoka, K. Watanabe, Y. Sakai, M. Sakamoto, J. Alloy. Compds. 224 (1995) 194–198.
[2] M.C. Navarro, E.V. Pannunzio-Miner, S. Pagola, M. Inés Gómez, R.E. Carbonio, J. Solid State Chem. 178 (2005) 847–854.
[3] W. Xiaoyu, Y. Yukawa, Y. Masuda, J. Alloy. Compds. 290 (1999) 85–90.
[4] P.K. Gallagher, B. Prescott, Inorg. Chem. 9 (1970) 2510–2512.
[5] J. Matt Farmer, D.F. Mullica, J.A. Kautz, J. Coord. Chem. 49 (2000) 325–333.
[6] X. Zhou, C.K. Duan, P.A. Tanner, J. Phys. Chem. Solids 69 (2008) 1038.
[7] Y. Masuda, K. Nagaoka, H. Ogawa, O. Nakazato, Y. Yukawa, H. Miyamoto, J. Alloy. Compds. 235 (1996) 23–29.
[8] W. Petter, V. Gramlich, F. Hulliger, J. Solid State Chem. 82 (1989) 161–167.
[9] D.F. Mullica, E.L. Sappenfield, Acta Crystallogr. C 47 (1991) 2433–2435.
[10] V. Gramlich, W. Petter, F. Hulliger, Acta Crystallogr. C 46 (1990) 724–726.
[11] A. Dommann, H. Vetsch, F. Hulliger, W. Petter, Acta Crystallogr. C 46 (1990) 1992–1994.
[12] P.A. Tanner, X. Zhou, W.T. Wong, C. Kratzer, H. Yersin, J. Phys. Chem. 110 (2006) 21386.
[13] D.F. Shriver, P.W. Atkins, C.H. Langford, Inorganic Chemistry, ELBS Oxford University Press, Oxford, 1991, p. 506.
[14] D.F. Mullica, E.L. Sappenfield, J. Solid State Chem. 82 (1989) 168–171.
[15] F. Hulliger, H. Vetsch, V. Gramlich, X.L. Xu, J. Alloy. Compds. 207 (208) (1994) 192–195.
[16] L.P. Zhang, X.J. Zhou, T.C.W. Mak, P.A. Tanner, Polyhedron 26 (2007) 4019–4023.
[17] B.M. Angelov, J. Phys. C: Solid State Phys. 10 (1977) L505–L507.
[18] D.F. Mullica, P.K. Hayward, E.L. Sappenfield, Acta Crystallogr. C 52 (1996) 61–63.
[19] T. Pretsch, K.W. Chapman, G.J. Halder, C.J. Kepert, Chem. Commun. (2006) 1857–1859.
[20] T.K. Panda, S. Randoll, C.G. Hrib, P.G. Jones, T. Bannenberg, M. Tamm, Chem. Commun. (2007) 5007–5009.
[21] D. Garcia, M. Faucher, J. Chem. Phys. 82 (1985) 5554–5564.
[22] A.J. Freeman, R.E. Watson, Phys. Rev. 127 (1962) 2058–2075.
[23] E. Clementi, C.C.J. Roothaan, M. Yoshimine, Phys. Rev. 127 (1962) 1618–1620.
[24] Q.W. Teng, S. Wu, J. Zhejiang Univ. Sci. 6B (2005) 602–605.
[25] E.A. Quadrelli, Inorg. Chem. 41 (2002) 167–169.
[26] J. Yao, B. Deng, L.J. Sherry, A.D. McFarland, D.E. Ellis, R.P. Van Duyne, J.A. Ibers, Inorg. Chem. 43 (2004) 7735–7740.